INTERNATIONAL JOURNAL OF CLIMATOLOGY
Int. J. Climatol. (2013)
Published online in Wiley Online Library
(wileyonlinelibrary.com) DOI: 10.1002/joc.3812

RMetS
Royal Meteorological Society

Southeastern Australian climate variability 1860–2009: a multivariate analysis

Linden Ashcroft,* David John Karoly and Joëlle Gergis

School of Earth Sciences, University of Melbourne, Australia

ABSTRACT: Historical datasets of instrumental temperature, rainfall and atmospheric pressure observations have recently been developed for southeastern Australia (SEA), extending the regional climate record back to 1860. In this study we use the newly extended datasets to conduct the first multivariate examination of SEA climatic changes from 1860 to 2009.

The climate in SEA is highly variable in response to fluctuations in large-scale circulation features including El Niño–Southern Oscillation (ENSO) and the Indian Ocean Dipole (IOD). To examine how teleconnection patterns in the SEA region have changed over time, we then applied a path analysis over the 1871–2009 period to isolate the independent relationships between SEA climate variables, ENSO and the IOD. The extended data revealed several relatively unknown periods of 19th century SEA climate variations. Cool and wet conditions were identified in the early parts of the 1860s, 1870s and 1890s, while dry conditions were found in the late 1870s, 1880–1885, and during the well-known Federation Drought (1895–1902).

Path analysis identified a decrease in the influence of ENSO on SEA rainfall during 1920–1959, particularly in the austral winter. Increasing correlations between the IOD and annual SEA rainfall and pressure were found in the recent 1970–2009 period, but appear to be within the range of natural variability in the context of the last 140 years. Despite large changes in the correlations between SEA rainfall, ENSO and the IOD, correlations between SEA rainfall and temperature remained stable over 1871–2009. Similar results were obtained using 20th Century Reanalysis data for 1871–2009, supporting the quality of the extended historical datasets and providing verification for the reanalysis data in SEA from the late 19th century.

KEY WORDS southeastern Australia; ENSO; IOD; climate variability; 19th century; climate; historical data

Received 13 December 2012; Revised 9 June 2013; Accepted 10 August 2013

1. Introduction

From 1997 to 2011, southeastern Australia (SEA) experienced the driest 13-year period followed by the wettest 2-year period since 1900 (Verdon-Kidd and Kiem, 2009; Timbal *et al.*, 2010; Australian Bureau of Meteorology, 2012). Both extremes had severe impacts across SEA, including water shortages, devastating floods and crop losses, all of which placed a large financial and psychological burden on regional and rural communities (Sartore *et al.*, 2008; Australian Bureau of Meteorology, 2012).

High rainfall variability is a feature of the SEA climate (Nicholls *et al.*, 1996a; Murphy and Timbal, 2008), and is influenced to a large extent by remote oceanic and atmospheric circulation patterns (Risbey *et al.*, 2009a). These include (1) El Niño–Southern Oscillation (ENSO) (McBride and Nicholls, 1983; Nicholls, 1988; Risbey *et al.*, 2009a), (2) Indian Ocean temperature fluctuations (represented by the Indian Ocean Dipole, IOD) (Saji *et al.*, 1999; Ashok and Guan, 2003; Murphy and Timbal, 2008; Risbey *et al.*, 2009a; Ummenhofer *et al.*, 2011), and (3) changes in mean sea level pressure (MSLP) over SEA caused by variations in the Southern Annular Mode (SAM) (Meneghini *et al.*, 2006; Hendon *et al.*, 2007) and the subtropical ridge (Drosdowsky, 2005; Larsen and Nicholls, 2009; Timbal and Drosdowsky, 2013).

These circulation features are not independent: ENSO and the IOD are known to interact through atmospheric teleconnection and common sea surface temperature (SST) patterns around Indonesia and the Maritime continent (Yu *et al.*, 2002; Behera and Yamagata, 2003; Meyers *et al.*, 2007; Risbey *et al.*, 2009a; Cai *et al.*, 2011). Negative IOD conditions do not normally occur during El Niño events, while positive IOD conditions are rare during La Niña events (Meyers *et al.*, 2007). ENSO and the IOD also affect MSLP over Australia through the direct response of tropical air to diabatic heating from SST anomalies, and indirectly through wave train development from tropical convection in areas of positive SST anomalies (Behera and Yamagata, 2003; Cai *et al.*, 2009, 2011).

Rainfall variations influenced by these large-scale circulation features in turn influence surface temperature changes. Maximum temperature (Tmax) is known to vary out-of-phase with rainfall, and minimum temperature (Tmin) generally varies in-phase, although

* Correspondence to: L. Ashcroft, School of Earth Sciences, University of Melbourne, VIC 3010, Australia. E-mail: l.ashcroft@student.unimelb.edu.au

this relationship exhibits high spatial variability (Power *et al.*, 1998; Jones, 1999; Jones and Trewin, 2000; Alexander *et al.*, 2007). Minimum temperatures are also influenced by maximum temperatures, particularly in the warmer months when Tmin values are determined by local night time cooling processes as well as the Tmax recorded the previous day (Jones and Trewin, 2000).

Recent interannual temperature variations related to rainfall across SEA have occurred against a backdrop of regional temperature increases (Trenberth *et al.*, 2007; Murphy and Timbal, 2008) which have been largely attributed to anthropogenic climate change (Karoly and Braganza, 2005). Mean temperatures across SEA have increased by almost 1 °C since 1960 (CSIRO and the Australian Bureau of Meteorology, 2012), and minimum temperatures are increasing at a greater rate than maximum temperatures (Alexander *et al.*, 2007; Ashcroft *et al.*, 2012; CSIRO and the Australian Bureau of Meteorology, 2012).

Given the highly variable nature of SEA rainfall, and the fundamental links between regional rainfall and temperature, it seems appropriate to examine the relationships between SEA temperature, rainfall and large-scale circulation features over time, particularly in the presence of recent warming trends. Unfortunately, the current long-term rainfall, MSLP and temperature datasets for Australia begin in 1900, 1907 and 1910, respectively (Lavery *et al.*, 1997; Alexander *et al.*, 2010; Trewin, 2013), restricting our ability to examine long-term changes in teleconnection patterns (Nicholls *et al.*, 1996a; Jones, 1999; Jones and Trewin, 2000). Furthermore, the first half of the 20th century is associated with a decrease in the variance of ENSO and the IOD (Karoly *et al.*, 1996; Kestin *et al.*, 1998; Reason *et al.*, 1998; Behera and Yamagata, 2003; Abram *et al.*, 2008) and a weakening of many global ENSO teleconnection patterns (e.g. Knippertz *et al.*, 2003). This may confound studies examining how anthropogenic climate change affects the influence of these features on the SEA climate.

To determine how background temperature increases may influence SEA climate variability, it is logical to instead compare SEA climate in recent decades with an earlier period of similar ENSO and IOD activity. Additionally, comparing periods of similar ENSO variance with an interval of lower ENSO variation, like the first half of the 20th century, may be valuable for understanding how the SEA climate responds to low-frequency changes in atmospheric and oceanic circulation.

This article examines changes in the relationships between ENSO, the IOD and the SEA climate using newly developed temperature, MSLP and rainfall datasets for SEA covering 1860–1909 (Ashcroft *et al.*, 2012; Gergis and Ashcroft, 2012), combined with existing high-quality datasets for 1910–2009. An additional 40 years of rainfall data (1860–1899), 47 years of MSLP data (1860–1906) and 50 years of temperature data (1860–1909) not only allows for a comparison between two periods of similar ENSO and IOD variance, but also provides more information on pre-1900 climate variations in SEA.

The article is structured as follows. Section 2 describes the newly extended datasets, including the homogenization process used to minimize the influence of non-climatic effects on the pre-1900 observations. Section 3 describes rainfall, temperature and MSLP changes for 1860–1909, including a comparison between MSLP over SEA and the intensity of the subtropical ridge intensity (STR-I). The observations are also compared to the 20th Century Reanalysis (20CR) dataset (Compo *et al.*, 2011) for the overlapping 1871–1909 period. Section 4 uses a path analysis (Schumacker and Lomax, 2004), calculating partial and semi-partial correlations to determine the dominant physical relationships between SEA temperature, rainfall, ENSO, the IOD and changes in MSLP. Relationships in the recent 1970–2009 period are compared to those during 1920–1959 (a time of reduced ENSO and IOD variance) and 1871–1909 (a period of similar ENSO variance to today), using both observational and 20CR data. Sections 5 and 6 discuss the results and present conclusions.

2. Data

Monthly Tmax, Tmin, rainfall (RAIN) and 9 am MSLP data for 1860–2009 were obtained from the Australian Bureau of Meteorology Australian Data Archive for Meteorology (Australian Bureau of Meteorology, 2000) for stations across SEA. For the purpose of this study, SEA is defined as the land within 136°–154°E and 26°–40°S (inset of Figure 1(a)), which includes the Australian states of Victoria and New South Wales, eastern South Australia and southern Queensland. Figure 1 shows the station networks for each variable, along with the decade in which observations begin at each station and the number of stations with data for each year from 1860 to 2009. Details of the temperature and rainfall networks are provided in Ashcroft *et al.* (2012) and Gergis and Ashcroft (2012), respectively. Stations were chosen for their temporal data availability during 1860–2009 and their spatial coverage over SEA.

Much of the pre-1900 temperature, rainfall and MSLP data have received little or no quality control (Lavery *et al.*, 1997; Alexander *et al.*, 2010; Ashcroft *et al.*, 2012; Trewin, 2013), so homogenization of the early data was crucial. Station history information, or metadata, were obtained for all stations from the Australian Bureau of Meteorology station history files and archives (see Ashcroft *et al.*, 2012 for details), to help identify possible changes to instrumentation, station location and observing practices. Due to data availability and the differences in spatial coherence of each variable, the homogenization of temperature, rainfall and MSLP datasets was conducted individually.

2.1. Temperature

Temperature observations are particularly sensitive to changes in observing location, instrumentation and

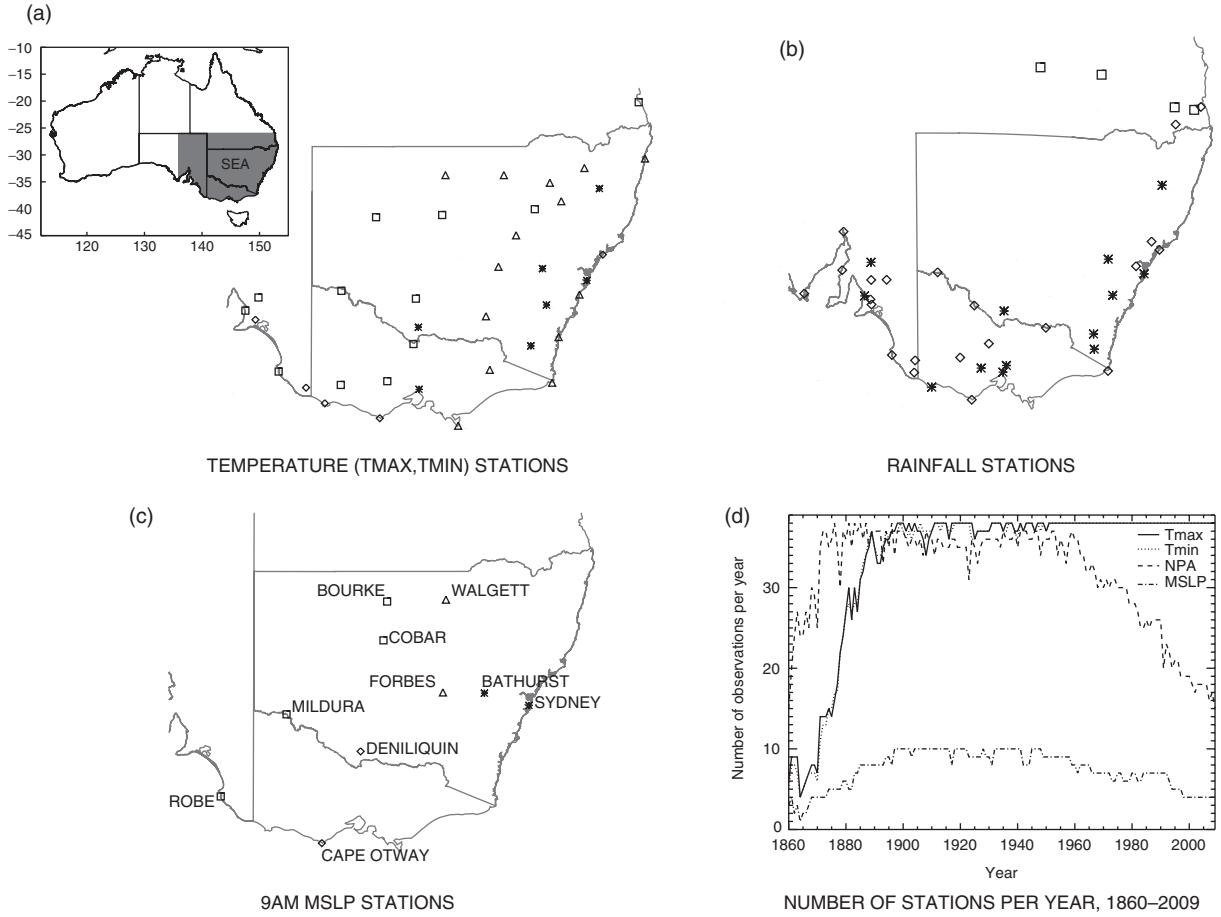

Figure 1. Stations in SEA used in this study observing maximum and minimum temperature (Tmax and Tmin, respectively, a), rainfall (RAIN, b) and 9 am mean sea level pressure (MSLP, c) over 1860–2009. Each station is marked to indicate the period in which observations began: pre–1860 (asterisk), 1860–1869 (diamond), 1870–1879 (triangle) and 1880–1900 (square). The number of stations with data in each network is also plotted (d). Note that for 1950–2009 TMAX and TMIN, data are provided by area-averages of SEA stations in the Australian Bureau of Meteorology high-quality ACORN-SAT dataset (Ashcroft *et al.*, 2012; Trewin, 2013). The inset of (a) shows the SEA region as defined in this study.

practice (Trewin, 2010). To minimize the influence of these changes, a two-step homogenization process was conducted on data from the 38 long-term temperature stations shown in Figure 1(a) using the statistical RHtestsV3 package (Wang *et al.*, 2007; Wang, 2008; Wang and Feng, 2010) and detailed station history information.

In Step 1, the penalized maximal F test from the RHtestsV3 package (Wang, 2008) was used to identify inhomogeneities in individual station data that were statistically significant or deemed to be significant in the presence of supporting metadata. In Step 2, reference series were built for each station using a weighted combination of the individually adjusted data from a subset of correlated neighbouring stations (Ashcroft *et al.*, 2012). The differences between data from each station and its reference series were examined for significant changes using the penalized maximal t test (Wang *et al.*, 2007) to further refine the adjustments made in Step 1.

Adjustments were applied to 1860–1950 temperature values alone (Ashcroft *et al.*, 2012) because the positive trend in the post-1950 record caused spurious trends in the early data when 1860–2009 data were examined together. A total of 185 (190) adjustments were identified for Tmax (Tmin) for 1860–1950, over half of which were supported by station history information (Ashcroft *et al.*, 2012). The homogenized Tmax and Tmin data for 1860–1950 were then combined with 1910–2009 SEA data from the Australian Bureau of Meteorology high-quality Australian Climate Observations Reference Network–Surface Air Temperature (ACORN–SAT) (Ashcroft *et al.*, 2012; Trewin, 2013). Annual and seasonal values of the homogenized network were highly correlated with the ACORN–SAT data during the overlapping 1910–1950 period (Pearson's correlation coefficient $r = 0.94$ for annual Tmax, $r = 0.85$ for annual Tmin, $r > 0.90$ for all seasonal values, p-value < 0.01 for all correlations).

2.2. Rainfall

A subset of 39 stations from the SEA rainfall network used in Gergis and Ashcroft (2012) was used to represent rainfall variation in SEA from 1860 to 2009. Log-transformed annual and monthly rainfall data were examined for changepoints using the penalized maximal

F test (Wang and Fang, 2010), and changepoints were compared to station metadata where possible. The high spatial variability of Australian rainfall and large year-to-year fluctuations (Nicholls *et al.*, 1996a) made inhomogeneities difficult to distinguish from real interannual changes so only 18 adjustments were made to data from 10 stations (see Gergis and Ashcroft, 2012).

2.3. Mean sea level pressure

The extended SEA MSLP network contained only 10 stations, but coverage was deemed sufficient due to the high spatial coherence between monthly and annual MSLP variations (Barring *et al.*, 1999; Hope *et al.*, 2010). Some gaps in the temporal coverage of available monthly MSLP data were found in 1917 and the early 1940s due to changes in the calculation of daylight savings time (B. Trewin, pers. comm.). These were filled using the monthly means of daily data from Alexander *et al.* (2010) wherever possible.

Initially, homogeneity adjustments were made in a similar way to the technique used for temperature (Section 2.1). However, adjusting the data from each station separately led to a large false positive trend being introduced to the pre-1900 data, due to the increase in MSLP that has occurred over Australia since the 1950s (Nicholls, 2010). Instead, the two-step homogenization process used for temperature data was applied to the MSLP data in reverse. Relative inhomogeneities were first identified for each station by comparing the data to a reference series built using a subset of between three and five highly correlated neighbouring stations. The high spatial coherence of monthly MSLP data meant large differences between data from individual stations and their reference series could easily be identified as inhomogeneities.

Additional inhomogeneities were then identified in the adjusted MSLP data by examining each station individually. The average annual MSLP values for the original and homogenized data are plotted in Figure 2, showing an improvement in the agreement between stations. The homogenization process greatly reduced the network's variability, reducing the impact of 72 inhomogeneities identified in the MSLP data. The majority of these inhomogeneities occurred before 1950 and were not supported by metadata.

2.4. Seasonally and regionally averaged data

Annual and seasonal anomalies of MSLP, Tmax and Tmin were calculated for 1860–2009 using the homogenized data for each station, relative to the 1910–1950 base period. Seasons were defined as austral summer (December–February, DJF), autumn (March–May, MAM), winter (June–August, JJA) and spring (September–November, SON). Note that summer values refer to the January and February of the year of interest ($t = 0$), and the December of the previous year ($t-1$). Rainfall totals for 1860–2009 were converted to normalized precipitation anomalies (NPAs) by subtracting the station mean and dividing by the standard deviation calculated over 1910–1950 base period (Wilks, 1995). NPAs were used instead of simple precipitation anomalies to remove the influence of the local variance on the regional average. RAIN is henceforth represented by NPAs.

Area-averages of annual and seasonal Tmax and Tmin anomalies as well as RAIN were calculated using Thiessen polygons (Thiessen, 1911) over the SEA region (Figure 1). A simple arithmetic average of the MSLP anomalies was used to represent MSLP variations due

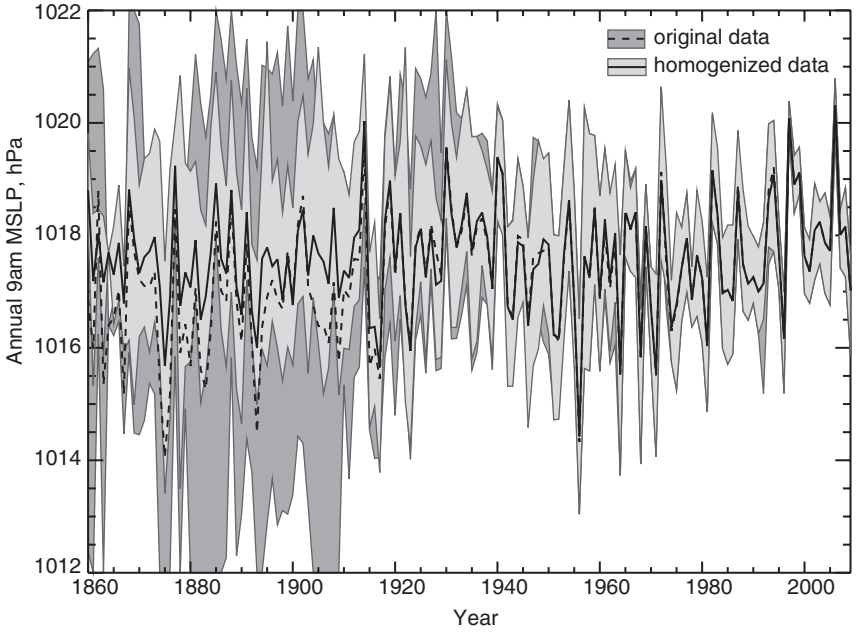

Figure 2. Average SEA MSLP calculated using homogenized data (solid black line) and original data (dashed black line) from the MSLP observational network (Figure 1(c)). The maximum and minimum MSLP values for each year are also plotted for the original data (dark grey shading) and homogenized data (light grey shading). See Section 2.3 for details of the homogenization process.

to the small network size. Note that while the rainfall stations used are clustered around the southern and eastern parts of the SEA region (Figure 1(b)), the area-average is still representative of the region as a whole. Correlations between the observational area-average and an average of gridded rainfall data over the full SEA region (Jones *et al.*, 2009) were high for the overlapping 1900–2009 period ($r > 0.88$ for seasonal and annual data, p-value < 0.01 for all correlations). A decrease in the number of rainfall stations in the post-1960 period (Figure 1(d)) did not have a large impact on the area-average either, with correlations remaining high ($r > 0.86$, p-value < 0.01) when the 1960–2009 period was examined separately.

The RAIN area-average was additionally in good agreement with Timbal and Fawcett (2012)'s study of rainfall variations in SEA for 1865–2010. Annual and seasonal correlations were greater than 0.8 during the overlapping period (p-value < 0.01), despite Timbal and Fawcett (2012) focussing on the southern part of SEA only and using a different data homogenization technique when developing their network. We are therefore confident that the rainfall area-average used here provides an adequate representation of rainfall variation across SEA.

2.5. Indices of ENSO, the IOD and STR intensity

The Niño 3.4 SST index (NINO3.4) was used to represent ENSO variations for 1871–2009. NINO3.4 was derived from the Hadley Centre Global Sea Ice and Sea Surface Temperature (HadISST) and National Centers for Environmental Prediction datasets (Reynolds and Smith, 1994; Rayner *et al.*, 2003; www.cgd.ucar.edu/cas/catalog/climind/TNI_N34/index.html). NINO3.4 is the 5-month smoothed normalized anomalies from the area-averaged SST over 170°W–120°W, 5°S–5°N (Trenberth, 1997; Trenberth and Stepaniak, 2001). Values less than −0.4 °C indicate La Niña conditions and values greater than 0.4 °C indicate El Niño conditions.

NINO3.4 was in good agreement with an extended Southern Oscillation Index (SOI) used to represent variations in the atmospheric component of ENSO for 1871–2010 ($0.66 \leq |r| \leq 0.83$ for seasonal data, $|r| = 0.80$ for annual data, p-value < 0.01 for all correlations) (Ropelewski and Jones, 1987; Allan *et al.*, 1991; Australian Bureau of Meteorology, 2011). Correlations were similar if the 1871–1900 period was examined alone ($0.51 \leq |r| \leq 0.81$ for seasonal data, $|r| = 0.78$ for annual data, p-value < 0.01 for all correlations). An SST-based index was used to represent ENSO here rather than the SOI, because the SOI (calculated as the difference between Tahiti and Darwin MSLP) is not independent of SEA MSLP variations (Nicholls, 2010).

Dipole Mode Index (DMI) values representing the IOD were calculated from the HadISST dataset for 1870–2009 using the KNMI Climate Explorer webpage (climexp.knmi.nl) (Saji *et al.*, 1999; Rayner *et al.*, 2003). The DMI is defined as the difference between SSTs in the western equatorial Indian Ocean (50°E–70°E, 10°N–10°S) and southeastern equatorial Indian Ocean (90°E–110°E, Equator–10°S) (Saji *et al.*, 1999). The DMI is normalized and has variability of periods longer than seven years removed to focus on interannual variability, as per Saji *et al.* (1999). Positive and negative IOD events are defined as years where the DMI is one standard deviation above or below the mean, respectively. An examination of the input data for HadISST showed that data coverage in the two boxes used to calculate the DMI is fair from at least 1880 onwards, with ships passing through the tropical Indian Ocean providing adequate pre-1900 SST data (Rayner *et al.*, 2003; Woodruff *et al.*, 2011).

An index of STR-I over SEA for 1890–2009 was provided by the Australian Bureau of Meteorology (W. Drosdowsky, pers. comm.). The STR is a belt of high pressure systems across the midlatitudes, particularly over eastern Australia, that corresponds to the descending branch of the Hadley Cell (Sturman and Tapper, 2004; Murphy and Timbal, 2008).

2.6. Twentieth Century Reanalysis data

To evaluate the results obtained using observational data, monthly estimates of Tmax, Tmin, RAIN and MSLP over SEA for 1871–2009 were derived from the 20CR dataset (Compo *et al.*, 2011). The 20CR is a reanalysis product developed using sub-daily surface pressure observations as input and observed monthly SSTs and sea ice conditions as boundary conditions (Compo *et al.*, 2011). Using the mean of a 56 member ensemble, 20CR provides a global atmospheric analysis every 6 hours on a $2^\circ \times 2^\circ$ grid from 1871 to 2009. For this study, area-averages of SEA Tmax, Tmin, RAIN and MSLP were calculated over 43 land grid boxes covering 138.75°E–151.875°E and 27.62°S–37.14°S. Area-averages were also calculated for each of the 56 individual ensembles, to provide an uncertainty estimate for the ensemble mean.

3. Temperature, rainfall and MSLP variations in SEA, 1860–2009

Figure 3(a) shows the annual variations of Tmax, Tmin, RAIN and MSLP from 1860 to 2009, while Figure 3(b) only shows variations from 1860 to 1909 relative to the 1860–1909 mean. Positive trends in Tmax, Tmin and MSLP since 1950 are clear in Figure 3(a), and have been discussed in detail in previous work (Torok and Nicholls, 1996; Della-Marta *et al.*, 2004; Nicholls, 2006; Trenberth *et al.*, 2007; Murphy and Timbal, 2008; Hope *et al.*, 2010; Nicholls, 2010; Ashcroft *et al.*, 2012; CSIRO and the Australian Bureau of Meteorology, 2012; Timbal and Drosdowsky, 2013). A small decrease in annual RAIN is apparent since 1950, which has been previously associated with a decline in cool season rainfall (Cai and Cowan, 2008; Risbey *et al.*; Nicholls, 2010).

Since variations in 20th century SEA climate have been discussed in detail in other studies, (e.g. Murphy and Timbal, 2008; Timbal *et al.*, 2010), the focus here is

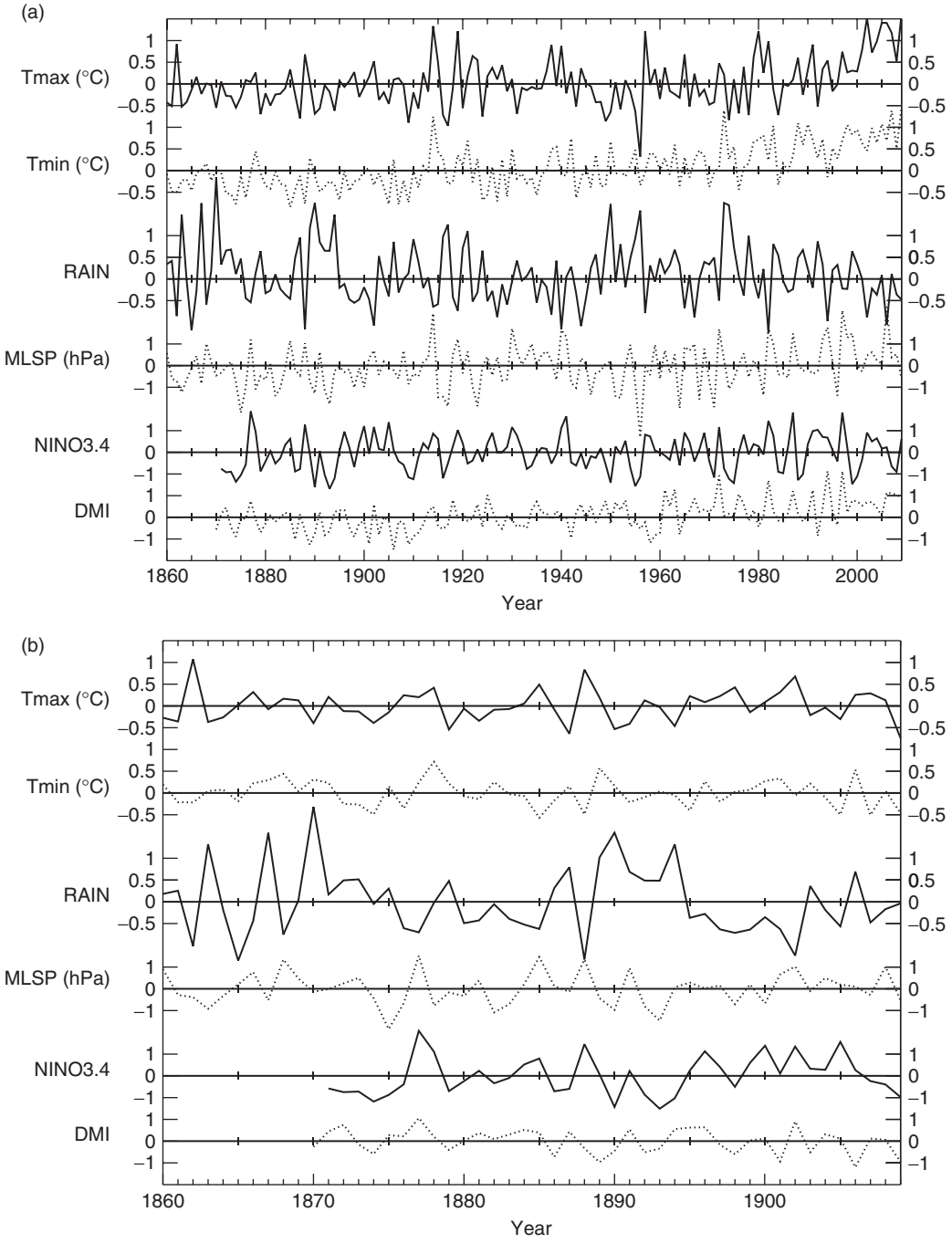

Figure 3. (a) Annual Tmax (°C), Tmin (°C), RAIN (normalized anomalies) and MSLP (hPa) across SEA as well as NINO3.4 and the DMI (normalized sea surface temperature difference) for 1860–2009. All anomalies have been calculated with respect to the 1910–1950 base period. (b) Annual Tmax (°C), Tmin (°C), RAIN (normalized anomalies) and MSLP (hPa) across SEA as well as NINO3.4 and the DMI (normalized sea surface temperature difference) for 1860–1909. Anomalies have been calculated with respect to the 1910–1950 base period and plotted relative to the 1860–1909 mean.

on climate variations in the newly extended 1860–1909 period. Table 1 shows years of warm and cool conditions in Tmax and Tmin for 1860–1909 compared to years of above or below-average RAIN and MSLP. Warm and cool years are defined as years with a Tmax or Tmin value half a standard deviation above or below the 1860–1909 mean. Years with above- or below-average RAIN and MSLP are defined in the same way. Standard deviations are calculated using 1860–1909 values only.

The 1860s were characterised by high interannual RAIN variability, with slightly cool Tmax and Tmin during 1860–1865 and warm conditions from 1866 to 1869. SEA experienced dry conditions in 1862, 1865–1866 and 1868, punctuated by very wet years in 1863 and 1867. The high Tmax value in 1862 and large rainfall variability in this first decade may be due to the reduced network in this earliest part of the record, although documentary historical evidence identified similar

Table 1. Summary of Tmax, Tmin, RAIN and MSLP conditions in SEA for 1860–1909. Warm (Cool) years are classified as years with a Tmax or Tmin value half a standard deviation above (below) the 1860–1909 mean. Wet (Dry) years are defined as years with a RAIN value half a standard deviation above (below) the 1860–1909 mean. Years with above- (below-) average MSLP (AA and BA respectively) are defined as years with an MSLP value half a standard deviation above (below) the 1860–1909 mean. Standard deviations are calculated over the 1860–1909 period. The ENSO classifications for each year from NINO3.4 and the IOD classifications from the DMI are also shown. EN represents an El Niño event, while LN represents a La Niña event. POS indicates a positive IOD event, NEG indicates a negative IOD event. A hyphen indicates normal ENSO and IOD conditions, and a blank cell means no data were available for that year. Conditions written in italics indicate cool and wet conditions, and features that are generally associated with wet conditions in SEA (below-average MSLP, La Niña and a negative IOD event). Text written in bold indicates warm, dry conditions and circulations features generally associated with dry conditions in SEA (above-average MSLP, El Niño and a positive IOD event).

Year	Tmax	Tmin	RAIN	MSLP	NINO3.4	DMI
1860	*Cool*	**Warm**	Normal	**AA**		
1861	*Cool*	*Cool*	Normal	Normal		
1862	**Warm**	*Cool*	**Dry**	*BA*		
1863	*Cool*	Normal	*Wet*	*BA*		
1864	*Cool*	Normal	Normal	Normal		
1865	Normal	*Cool*	**Dry**	Normal		
1866	**Warm**	**Warm**	**Dry**	**AA**		
1867	Normal	**Warm**	*Wet*	*BA*		
1868	Normal	**Warm**	**Dry**	**AA**		
1869	Normal	Normal	Normal	**AA**		
1870	*Cool*	**Warm**	*Wet*	Normal		
1871	**Warm**	**Warm**	Normal	Normal	*LN*	-
1872	Normal	*Cool*	*Wet*	Normal	*LN*	**POS**
1873	Normal	*Cool*	*Wet*	**AA**	*LN*	-
1874	*Cool*	*Cool*	Normal	*BA*	*LN*	*NEG*
1875	Normal	**Warm**	Normal	*BA*	*LN*	-
1876	**Warm**	*Cool*	**Dry**	*BA*	*LN*	-
1877	**Warm**	**Warm**	**Dry**	**AA**	**EN**	**POS**
1878	**Warm**	**Warm**	Normal	*BA*	**EN**	-
1879	*Cool*	**Warm**	*Wet*	Normal	*LN*	-
1880	Normal	Normal	**Dry**	Normal	-	-
1881	*Cool*	Normal	**Dry**	**AA**	-	-
1882	Normal	**Warm**	Normal	*BA*	-	-
1883	Normal	Normal	**Dry**	*BA*	-	-
1884	Normal	Normal	**Dry**	Normal	**EN**	-
1885	**Warm**	*Cool*	**Dry**	**AA**	**EN**	-
1886	Normal	*Cool*	Normal	Normal	*LN*	*NEG*
1887	*Cool*	**Warm**	*Wet*	Normal	*LN*	-
1888	**Warm**	*Cool*	**Dry**	**AA**	**EN**	-
1889	**Warm**	**Warm**	*Wet*	*BA*	-	*NEG*
1890	*Cool*	**Warm**	*Wet*	*BA*	*LN*	-
1891	*Cool*	*Cool*	*Wet*	**AA**	-	-
1892	Normal	Normal	*Wet*	*BA*	*LN*	-
1893	Normal	Normal	*Wet*	*BA*	*LN*	-
1894	*Cool*	Normal	*Wet*	Normal	*LN*	-
1895	**Warm**	*Cool*	Normal	Normal	-	**POS**
1896	Normal	**Warm**	Normal	Normal	**EN**	**POS**
1897	**Warm**	*Cool*	**Dry**	Normal	**EN**	-
1898	**Warm**	Normal	**Dry**	*BA*	*LN*	*NEG*
1899	Normal	Normal	**Dry**	Normal	**EN**	-
1900	Normal	**Warm**	Normal	*BA*	**EN**	-
1901	**Warm**	**Warm**	**Dry**	**AA**	-	*NEG*
1902	**Warm**	Normal	**Dry**	**AA**	**EN**	**POS**
1903	*Cool*	**Warm**	Normal	Normal	-	-
1904	Normal	Normal	Normal	**AA**	-	-
1905	*Cool*	*Cool*	**Dry**	Normal	**EN**	-
1906	**Warm**	**Warm**	*Wet*	Normal	-	*NEG*
1907	**Warm**	*Cool*	**Dry**	Normal	-	-
1908	Normal	Normal	Normal	**AA**	*LN*	-
1909	*Cool*	*Cool*	Normal	*BA*	*LN*	*NEG*

periods of wet and dry conditions across the SEA region (Garden, 2009). Wet years were generally associated with a decrease in MSLP, while dry years experienced an increase. A palaeoclimate ENSO reconstruction (Gergis and Fowler, 2009) identified 1860–1864 and 1867 as La Niña years, while 1865, 1866 and 1868 experienced El Niño conditions. The years 1866 and 1868 in particularly were subject to strong El Niño events, and as El Nino conditions are generally associated with below-average rainfall in SEA (Murphy and Timbal, 2008), this provides further support for the rainfall variations found during these years (Garden, 2009; Gergis and Fowler, 2009).

SEA experienced wet conditions in the first half of the 1870s associated with several La Niña events (Gergis and Fowler, 2009; Ummenhofer *et al.*, 2011). The year 1879 was also characterised by wet and cool conditions under the influence of a La Niña phase of ENSO. Wet years were generally associated with normal to cool Tmax and normal to below-average MSLP values. Tmin values were above-average during 1870 and 1871, indicating the influence of increased cloud cover on trapping outgoing longwave radiation at night (Power *et al.*, 1998; Jones and Trewin, 2000). In 1872–1874, however, cool Tmin conditions were experienced due to wetter conditions in the warmer months when Tmin was also influenced by cooler than normal Tmax conditions (seasonal analysis not shown). The 1876–1878 period was dominated by warm and dry conditions. The strong 1877 El Niño event in particular was associated with very dry conditions during DJF and JJA, resulting in warm Tmax and Tmin values and above-average MSLP.

A moderate but prolonged drought influenced SEA from 1880 to 1885, and was associated with generally average temperatures. Only 1885 experienced an increase in Tmax and a simultaneous drop in Tmin, associated with the driest year of the drought (Figure 3(b)) and a peak in MSLP anomalies. Interestingly, the NINO3.4 index in Table 1, as well as an independent ENSO index developed by Ummenhofer *et al.* (2011), suggest that there was a lack of El Niño conditions during this dry period, with El Niño events only identified in 1884 and 1885 using NINO3.4. The Southern Oscillation Index on the other hand (not shown) was negative in 1881, 1882, 1884 and 1885 (Gergis and Fowler, 2005; Australian Bureau of Meteorology, 2011), indicating atmospheric conditions generally associated with El Niño events. This suggests that there may have been some decoupling of the oceanic and atmospheric components of ENSO during the first half of the 1880s (Trenberth, 1997; Gergis and Fowler, 2005).

The second half of the 1880s was characterised by high interannual rainfall and temperature variability, largely associated with both phases of ENSO. Wet and cool Tmax conditions in 1887 occurred during a La Niña event, while 1888 stands out as a particularly dry year with high MSLP values, very warm Tmax values and cold Tmin conditions in association with a strong El Niño event. The lack of rain in 1888 had widespread agricultural and economic repercussions, and became known as the Centennial Drought (Nicholls, 1995).

Wet conditions prevailed from 1889 to 1894, associated with another series of La Niña events. Slightly cool Tmax conditions were experienced, and generally average Tmin values. It is interesting to note that positive IOD events were reported by Ummenhofer *et al.* (2011) during the wet years 1891 and 1894, although positive IOD conditions are generally associated with dry conditions in SEA (Meyers *et al.*, 2007; Ummenhofer *et al.*, 2011). This disagreement may be because the IOD years identified by Ummenhofer *et al.* (2011) cover June–December, when upwelling occurs of the Indonesian coast (Meyers *et al.*, 2007), rather than the complete calendar year. It could also be that the positive rainfall anomalies were only experienced in the northern part of SEA where the IOD influence is weaker (Risbey *et al.*, 2009a), although preliminary spatial analysis (not shown) suggests that this was not the case.

The Federation Drought (named after the Federation of Australia in 1901) occurred from 1895 to 1902, with extended dry conditions, warm Tmax values and varying Tmin values. El Niño events dominated during 1895–1902, consistent with the findings of Verdon-Kidd and Kiem (2009) that the Federation Drought was associated with a prolonged El Niño phase. Positive IOD events also occurred in 1896 and 1902, in conjunction with El Niño. MSLP values remained almost constantly average during this period, only increasing in 1901–1902 during the driest years of the drought. The 1905–1910 period marked a return to high interannual variability across SEA. Negative IOD events and La Niñas were associated with wet and warm conditions in 1906 and cool conditions in Tmax and Tmin in 1909.

Figure 3 shows that MSLP values over 1860–2009 varied largely out-of-phase with SEA rainfall. A comparison between the annual and seasonal MSLP averages and the STR-I over 1890–2009 is shown in Table 2. The level of agreement is very high for annual, JJA, SON and MAM, although not quite as high for summer when the STR is at its southernmost location (Drosdowsky, 2005). Annual variations in MSLP can therefore be considered

Table 2. Pearson's correlation coefficients (r) between the SEA annual and seasonal (austral summer, DJF; autumn, MAM; winter, JJA; and spring, SON) average 9 am MSLP and the intensity of the STR (Drosdowsky, 2005), 1890–2009. All correlations are statistically significant (p-value < 0.05, significant using the two-tailed Student's t-test). Correlations between year-to-year differences are also given in brackets.

	ANN	DJF	MAM	JJA	SON
$r_{\text{STR-I MSLP}}$	0.89 (0.93)	0.81 (0.87)	0.91 (0.94)	0.93 (0.96)	0.94 (0.95)

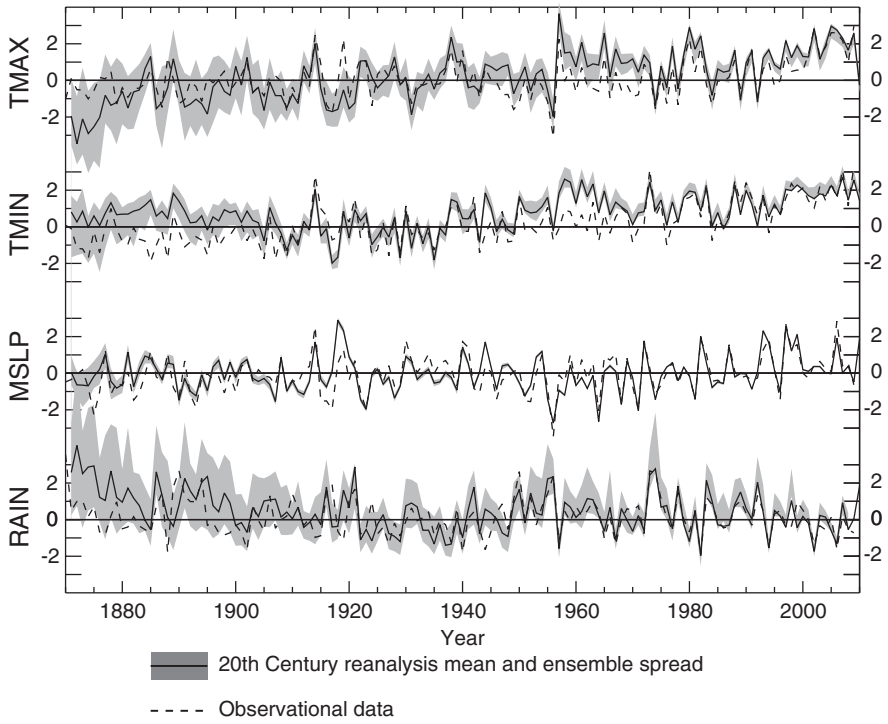

Figure 4. Annual Tmax (°C), Tmin(°C), MSLP (hPa) and RAIN (normalized anomalies) anomalies across SEA for 1871–2009 calculated using 20CR gridded data (solid lines) and area-averaged observational data (dashed lines). Anomalies have been calculated and normalized relative to the 1910–1950 base period. The annual maximum and minimum anomalies for each variable across the 56 ensemble members of the 20CR are also plotted (grey shading) to provide an estimate of 20CR uncertainty.

a measure of variations in the STR-I, particularly in the cooler seasons. MSLP, DMI and NINO3.4 appear largely in-phase, with positive MSLP anomalies being associated with positive IOD and El Niño conditions.

3.1. Comparison with 20CR reanalysis

Figure 4 compares the normalized annual values of SEA Tmax, Tmin, RAIN and MSLP determined by the 20CR over 1871–2009 with that of the extended observational SEA data, while Table 3 provides the correlations between the observational and reanalysis datasets. Correlations are shown between original data values as well as year-to-year differences. Year-to-year differences were examined to determine the ability of the 20CR to capture interannual variability over SEA, rather than long-term changes in the mean.

Correlations between the 20CR dataset and the extended SEA observations are high, particularly for MSLP and over the 20th century. The high agreement for MSLP is not surprising, as the number of stations with early MSLP data in SEA is small and several stations in the observational network have also been used in the 20CR (R. Allan, pers. comm.). The high correlations do, however, provide verification of the homogenization technique used to develop the extended observational MSLP network (Section 2.3). While Tmax values from the 20CR are almost 2 °C lower than the observations before 1880, and Tmin values are around 1 °C higher, the year-to-year variations are similar to the observations. These results suggest that the 20CR can represent relative variations in interannual SEA temperature during 1871–1909, but not the absolute value for each year.

RAIN values are also much higher in the 20CR than the observed SEA RAIN until about 1885, although the ensemble spread shows that the observational data are within the range of 20CR uncertainty. This discrepancy between the 20CR and observational data before 1885 may be due to a lack of available SST and MSLP data around SEA in this early period, or due to the interpolation techniques used in the early part of the

Table 3. Annual and seasonal correlations between the mean 20CR SEA area-average and the observational data area-average for Tmax, Tmin, RAIN and MSLP, 1871–2009. All correlations are statistically significant (p-value < 0.05, significant using the two-tailed Student's t-test). Correlations between year-to-year differences are also given in brackets.

	ANN	DJF	MAM	JJA	SON
Tmax	0.71 (0.79)	0.60 (0.79)	0.73 (0.73)	0.83 (0.86)	0.79 (0.81)
Tmin	0.71 (0.82)	0.77 (0.78)	0.69 (0.82)	0.72 (0.76)	0.74 (0.81)
RAIN	0.59 (0.57)	0.51 (0.62)	0.69 (0.64)	0.63 (0.64)	0.63 (0.67)
MSLP	0.78 (0.87)	0.66 (0.78)	0.85 (0.88)	0.91 (0.95)	0.83 (0.87)

reanalysis (Rayner *et al.*, 2003; Compo *et al.*, 2011). Despite differences in the mean, the year-to-year rainfall variations are similar. Interestingly, the high rainfall in the 20CR data from 1871 to 1885 is associated with lower Tmax. While there may be issues with the first decade or so of the 20CR data, this result shows the ability of the reanalysis to reproduce SEA's strong physical out-of-phase relationship between Tmax and rainfall.

This examination of pre-1910 SEA climate has demonstrated that there is a high level of covariation between SEA temperature, rainfall, MSLP, ENSO and the IOD. There are also similarities between the second half of the 19th century and the second half of the 20th century. For example, the early 1870s and 1890s stand out as prolonged periods of above-average rainfall, similar to the 1950s and 1970s. Conversely, the early 1880s and Federation Drought are important below-average rainfall periods that need to be placed into context in relation to the 1997–2009 'Big Dry' (Verdon-Kidd and Kiem, 2009). One way to explore these periods is to look at the relationships between climatic variables and see how they vary over time. To allow direct comparison between the 20CR and SEA observational datasets, the remaining analysis will focus on the 1871–2009 period of overlap.

4. Climate covariations, 1871–2009

Figure 5 presents the annual and seasonal Pearson's correlation coefficients (r) between SEA Tmax, Tmin and RAIN, and between large-scale circulation features NINO3.4, DMI and MSLP and RAIN for 1871–2009. Figure 5 also shows scatterplots to visually represent the relationships between each variable. Statistical significance thresholds were determined using a 2000-member Monte Carlo simulation ensemble (Livezey and Chen, 1983), where correlations were calculated between 2000 estimates from lag-1 autoregressive models forced with the same autocorrelation as the observational data. This produced a probability density function for each correlation, with significance levels taken at the 5th and 95th percentiles. To minimize the influence of the post-1950 positive trends in the MSLP and temperature (Nicholls, 2010), correlations were calculated between the year-to-year differences of each variable, although the results were comparable if this step was omitted.

The SEA temperature–rainfall relationships show clear seasonal variations. In the warmer seasons (austral summer, DJF and spring, SON), Tmax and Tmin are highly correlated, indicating that Tmin is primarily influenced by Tmax (Jones and Trewin, 2000). Conversely, the Tmin–RAIN relationship is weakest during DJF and SON. In austral autumn and winter (MAM and JJA) this relationship reverses: RAIN becomes the dominant influence on Tmin, and the Tmax–Tmin relationship is at its weakest. The negative Tmax–RAIN relationship remains fairly constant throughout the year, and is slightly stronger during JJA and SON.

The climatic influences on rainfall also show distinct seasonal differences, reflecting the strong relationships

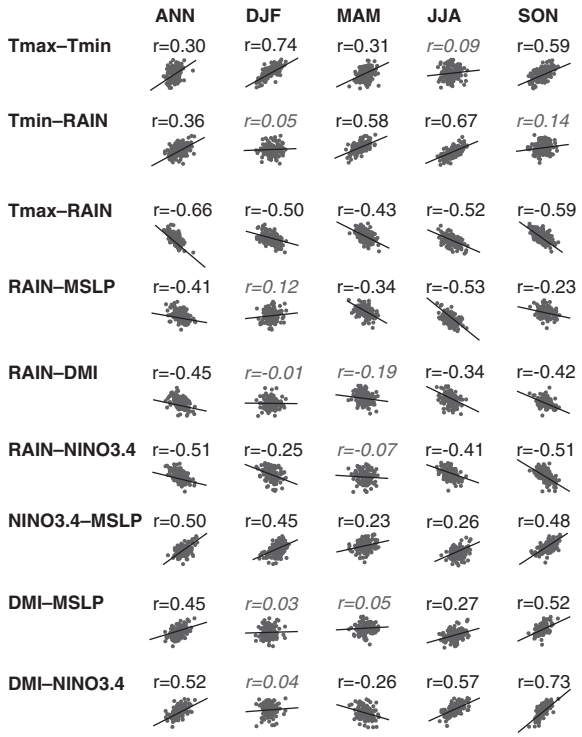

Figure 5. Pearson's correlation coefficients (r) between annual and seasonal SEA Tmax, Tmin and RAIN, and SEA RAIN and NINO3.4, DMI and MSLP, 1871–2009. Correlations that are statistically significant (determined using a 2000-member Monte Carlo test) are printed in black, and non-significant correlations are printed in grey italics. Scatterplots between normalized variables are also plotted as visual representations of the correlations.

between SEA rainfall, ENSO and the IOD during the austral winter and spring (Risbey *et al.*, 2009a). MSLP has the greatest impact on SEA rainfall during JJA when it is a good proxy for the STR-I (Table 2). The negative DMI–RAIN relationship is only significant during JJA and SON, while the NINO3.4–RAIN relationship is significant during all seasons except MAM. This is to be expected as autumn is a well-known period of poor ENSO and IOD climate modulation in Australia (McBride and Nicholls, 1983; Murphy and Timbal, 2008). NINO3.4 shows a consistent positive relationship with the MSLP throughout the year, with the weakest relationship in MAM. The DMI is also positively correlated with the MSLP, but the relationship is only significant during JJA and SON. The positive DMI–NINO3.4 relationship is also greatest during these cooler seasons, when the IOD is most active (Saji *et al.*, 1999).

These relationships show how SEA temperature, rainfall, MSLP and large-scale circulation features interact, but do not take into account the interdependencies amongst them. The high DMI–RAIN correlations in JJA and SON, for example, may be enhanced by the additional influence of the MSLP, which is positively correlated with the DMI during this time. Conversely, the Tmin–RAIN relationship during DJF and MAM might be weakened by the additional influence of Tmax on Tmin that is known to occur during these seasons (Jones and Trewin, 2000).

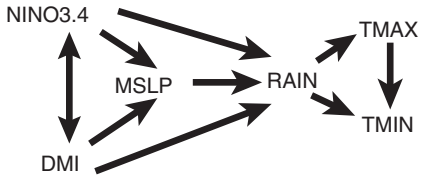

Figure 6. Schematic of the key dynamic relationships between SEA temperature (Tmax and Tmin), rainfall (RAIN), MSLP and large-scale circulation features (ENSO represented by NINO3.4 and the IOD represented by the DMI). See Section 4 for details.

To examine such interactions, Figure 6 presents a schematic of the dominant physical relationships between large-scale circulation features and SEA climate variables on interannual and seasonal scales. ENSO (represented by NINO3.4) and the IOD (represented by the DMI) influence each other (Yu *et al.*, 2002; Behera and Yamagata, 2003; Meyers *et al.*, 2007; Cai *et al.*, 2011) and the surface pressure over SEA (Behera and Yamagata, 2003; Cai *et al.*, 2011). All three of these circulation features affect SEA rainfall (Murphy and Timbal, 2008). Rainfall variations affect Tmax and Tmin (Jones, 1999; Jones and Trewin, 2000; Alexander *et al.*, 2007). Tmax has an additional impact on Tmin, but Tmin does not have a major influence on Tmax (Jones and Trewin, 2000).

Several studies have also identified significant relationships between SEA temperatures and large-scale circulation features (Halpert and Ropelewski, 1992; Nicholls *et al.*, 1996b; Power *et al.*, 1998; Jones and Trewin, 2000 for ENSO; Saji and Yamagata, 2003 for IOD; Gillett *et al.*, 2006; Hendon *et al.*, 2007 for MSLP). However, the majority of the influence of these features on SEA temperature comes from the modulation of radiant and latent surface heat fluxes, which is driven by changes in rainfall and cloud cover (Power *et al.*, 1998; Jones, 1999; Jones and Trewin, 2000). Therefore, temperature variations were only examined in relation to coincident rainfall variability, because it represents the most significant influence on interannual temperature changes in SEA.

To isolate the independent influences on SEA rainfall, temperature, and MSLP, a path analysis is applied, using partial and semi-partial correlations (Schumacker and Lomax, 2004). Partial correlations quantify the strength of a statistical relationship between the residuals of two variables, once the influence of an external variable (or set of variables) is removed from both. For example, to determine how Tmax is related to Tmin, we first need to remove the influence of RAIN on both variables by calculating a linear regression between Tmax and RAIN, and Tmin and RAIN. Subtracting the regressions from Tmax and Tmin leaves the residuals, or the components of Tmin and Tmax that are not influenced by RAIN. The correlation between these residuals is the partial correlation, and is represented by $r_{TminTmax.RAIN}$. Semi-partial correlations work in a similar way, but the external influence of another variable is only removed from one of the variables of interest rather than both. In the case of Tmin and RAIN for example, we only need to remove the influence of Tmax on Tmin, because Tmax does not have a physical effect on RAIN. This is represented by $r_{RAIN(Tmin.Tmax)}$.

Figure 7 presents the partial and semipartial correlations between each variable relevant to SEA climate, taking into account the influence of the relationships plotted in Figure 6. Scatterplots between residuals are shown, as well as schematics similar to Figure 6, with the width of each arrow indicating the relative strength of the correlations between variables. Correlations are calculated between year-to-year differences, to minimize the influence of trends in the post-1950 data, and a 2000-member Monte Carlo simulation ensemble determines statistical significance.

By using partial and semipartial correlations, the independent relationships between the SEA climate and large-scale circulation are extracted. RAIN influences Tmin throughout the year, not just in the cooler months as suggested by Figure 5. The Tmax–Tmin relationship is also highly positive throughout the year, although remains slightly stronger in DJF and MAM. MSLP is positively correlated with RAIN during DJF if the influences of DMI and NINO3.4 are removed, and remains significantly negatively correlated during MAM and JJA. The DMI–RAIN relationship breaks down in all seasons with the influence of MSLP and NINO3.4 removed, although there is still a weakly significant relationship on an annual scale. The NINO3.4–RAIN relationship remains statistically significant for all seasons except MAM, similar to the results of the regular correlation analysis shown in Figure 5.

The relationship between NINO3.4 and MSLP weakens slightly when the influence of the DMI is removed, particularly during JJA and SON. The DMI–MSLP relationship also weakens when the influence of NINO3.4 is removed, especially in JJA. Interestingly, the DMI–MSLP relationship during SON is significant, but the DMI–RAIN correlation is not. This suggests that the DMI influence on SEA rainfall during SON comes through remote modulation of the local MSLP, as discussed by Cai *et al.* (2011).

Repeating the analysis using 20CR data (not shown) revealed similar relationships, although correlations were generally slightly lower than those obtained using observational data. Two exceptions were the Tmax–Tmin correlations, which were around 0.1 higher using the 20CR data in both annual and seasonal analysis, and the annual NINO3.4–RAIN relationship, which was much weaker when using 20CR rainfall. This was also the case when 20CR relationships were examined using regular correlations rather than path analysis.

4.1. Covariations in subperiods: 1871–1909, 1920–1959 and 1970–2009

Having identified the key relationships between SEA climate variables and large-scale oceanic and atmospheric influences, we now examine how they differ in three subperiods: 1871–1909, 1920–1959 and 1970–2009.

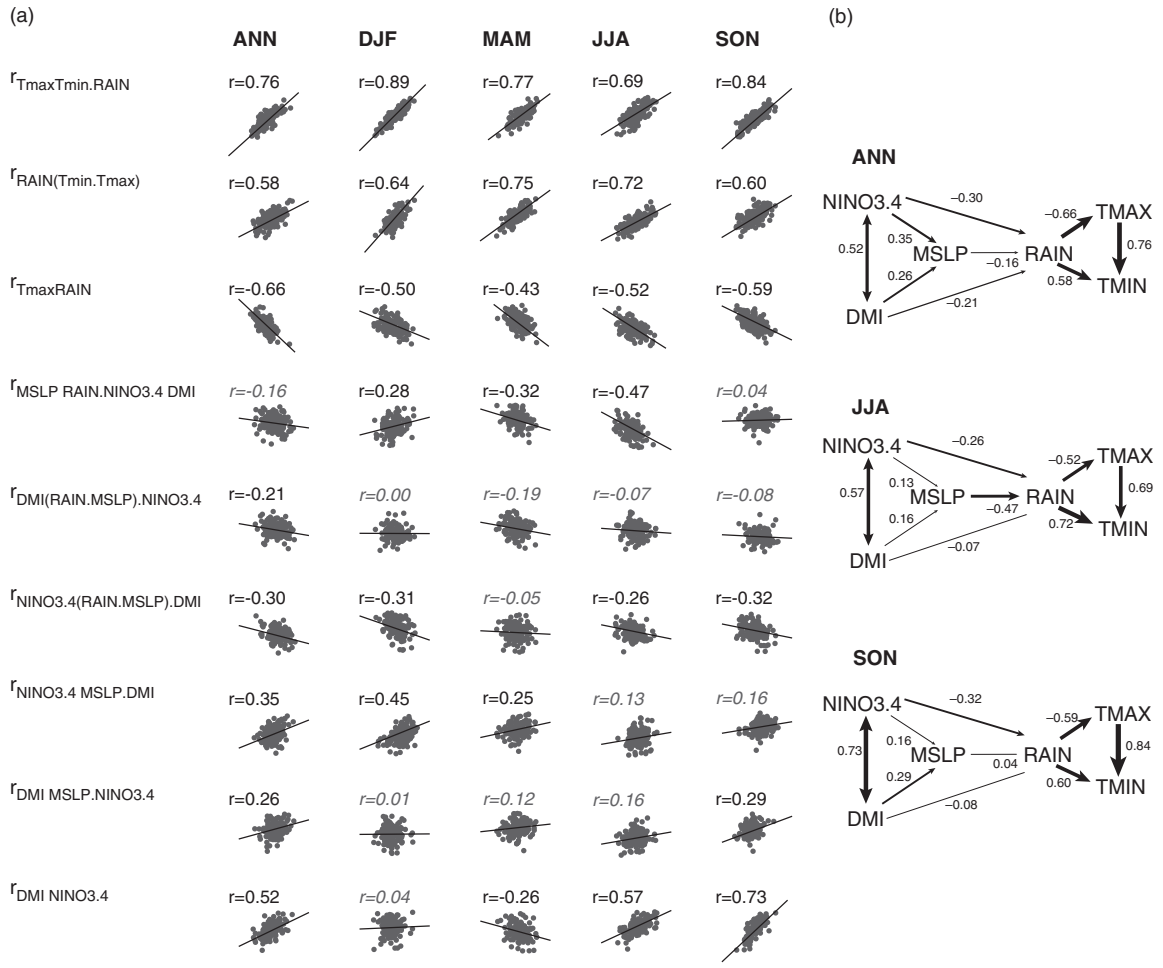

Figure 7. (a) Correlations between annual and seasonal Tmax, Tmin and RAIN, and RAIN, NINO3.4, DMI and MSLP, 1871–2009. Correlations have been calculated for each relationship represented by an arrow in Figure 6. $r_{AB.C}$ indicates a partial correlation between A and B, removing the influence of C from both A and B, and $r_{AB.CD}$ means that the influence of both C and D have been removed from A and B before calculation. $r_{A(B.C)}$ indicates a semi-partial correlation, removing the influence of C from B before calculation. r_{AB} indicates a simple Pearson's correlation coefficient between A and B. $r_{A(B.C).D}$ means that the linear influence of C on B has been removed, and then the influence of D on A and the B residuals has also been removed before calculation. Correlations that are statistically significant (determined using a 2000-member Monte Carlo test) are printed in black, and non-significant correlations are printed in grey italics. (b) Annual, JJA and SON correlations from (a) replotted using the schematic shown in Figure 6. Arrow width is an indication of the correlation strength between each variable.

We choose these subperiods to examine the influence of ENSO variance and background warming on the relationships affecting SEA climate. In 1871–1909 and 1970–2009 the ENSO variance is similar (Kestin *et al.*, 1998), but only 1970–2009 is influenced by significant regional warming (CSIRO and the Australian Bureau of Meteorology, 2012; Jones *et al.*, 2012). The 1920–1959 period is not subject to large-scale warming, but experiences a drop in the variance of ENSO and the IOD compared to the other two subperiods (Kestin *et al.*, 1998; Abram *et al.*, 2008). The 1910–1919 and 1960–1970 periods have been identified as times of large changes in ENSO variance (Kestin *et al.*, 1998). To concentrate on stable periods of different ENSO conditions and minimise the influence that these rapid variance changes might have on the analysis, these decades have been omitted from the subperiod comparison. We also limit our focus to JJA and SON, as ENSO and the IOD have the greatest influence on SEA rainfall during this time of the year (Risbey *et al.*, 2009a).

Table 4 shows the regular correlations between SEA RAIN, the NINO3.4 and DMI for each of the different subperiods, as well as the full 1871–2009 period. The standard deviations of the DMI and NINO3.4 in each subperiod are also shown. The standard deviations show a clear drop in annual, JJA and SON variability in ENSO during 1920–1959, with a corresponding decrease in the NINO3.4–RAIN correlations. The DMI standard deviation does not drop to the same extent, and in fact seems to be increasing with time, in agreement with studies of long-term IOD variations (Ihara *et al.*, 2008). The only real exception to this occurs in SON during 1920–1959, where there is a decrease in the DMI standard deviation and a small drop in the DMI–RAIN correlation.

To further examine the dynamics behind these low-frequency changes in the relationships between the DMI, NINO3.4 and SEA climate, Figure 8 shows schematics of the annual, JJA and SON correlations between climate variables in each subperiod using the

Table 4. Annual (ANN), austral winter (JJA) and austral spring (SON) correlations between NINO3.4 and RAIN ($r_{NINO3.4\text{-}RAIN}$) and the DMI and RAIN ($r_{DMI\text{-}RAIN}$) during 1871–2009, 1871–1909, 1920–1959 and 1970–2009. Statistically significant correlations are printed in bold (p-value < 0.05, significant using the two-tailed Student's t-test). The standard deviation of NINO3.4 and the DMI for each season and period or subperiod is also given (SD NINO3.4 and SD DMI).

	1871–2009			1871–1909			1920–1959			1971–2009		
	ANN	JJA	SON	ANN	JJA	SON	ANN	JJA	SON	ANN	JJA	SON
$r_{NINO3.4\text{-}RAIN}$	**−0.51**	**−0.41**	**−0.51**	**−0.54**	**−0.61**	**−0.61**	**−0.49**	−0.16	**−0.44**	**−0.57**	**−0.54**	**−0.46**
$r_{DMI\text{-}RAIN}$	**−0.45**	**−0.34**	**−0.42**	−0.33	−0.33	**−0.46**	**−0.43**	**−0.40**	−0.34	**−0.66**	**−0.39**	**−0.39**
SD NINO3.4	0.81	0.82	1.15	0.89	0.88	1.20	0.69	0.68	0.91	0.90	0.92	1.38
SD DMI	0.67	1.05	1.20	0.56	0.89	1.07	0.50	0.90	0.89	0.69	1.14	1.30

path analysis outlined in the previous section. A block bootstrapping technique was used (Zwiers *et al.*, 2011) to determine if the correlations identified were significantly different from what is to be expected from a random 40-year period between 1871 and 2009. Eight five-year blocks were chosen at random from the observational time series and pieced together to form a synthetic 40-year time series for each variable. For the 39-year period 1871–1909, a synthetic 39-year time series was compiled using 13 three-year blocks, although the results obtained were very similar to the 40-year series. Path analysis was then conducted between these time series 2000 times to create probability density functions, with significance levels taken at the 5th and 95th percentiles. Correlations that are significantly different from expected are printed in bold italics in Figure 8.

The greatest influence on RAIN during the 1871–1909 subperiod came from NINO3.4, with no significant correlations between RAIN and the DMI and weak correlations between RAIN and MSLP. The JJA MSLP–RAIN correlation was substantially weaker than for 1871–2009, perhaps due to quality issues in the MSLP data, although 20CR correlations (not shown) reported a similarly weak relationship. RAIN was positively correlated with MSLP during SON, possibly reflecting the positive influence of the STR-I on eastern seaboard rainfall identified by Timbal and Drosdowsky (2013). MSLP was also positively correlated with the DMI during SON in this first subperiod, equivalent to the full 1871–2009 correlation shown in Figure 7.

The main influences on RAIN during 1920–1959 were local MSLP variations and the DMI, as the influence of NINO3.4 on RAIN weakened dramatically. The influence of NINO3.4 on RAIN and MSLP was weaker during 1920–1959 than during any other time period examined. Conversely, the annual and JJA MSLP–RAIN relationships were stronger during this period than at any other time period considered. In the cooler seasons, this represented strong negative correlations between the STR-I and SEA rainfall. The SAM may have also been associated with the high MSLP–RAIN correlations during 1920–1959, as variations in the SAM are closely linked to MSLP changes in southern SEA (Risbey *et al.*, 2009a).This relationship is beyond the scope of this study. The DMI–RAIN relationship was significantly negative during 1920–1959, and there was also a weak but significant negative relationship between annual DMI and MSLP.

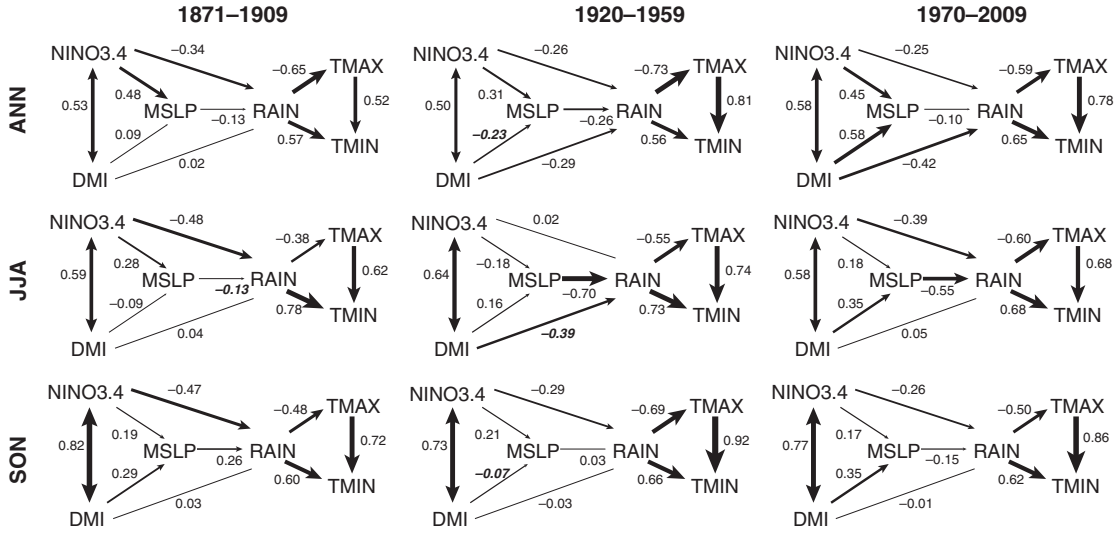

Figure 8. Correlations between SEA climate variables (Tmax, Tmin, RAIN and MSLP) and large-scale circulation features (NINO3.4 and DMI) over 1871–1909, 1920–1959 and 1970–2009 for annual values (ANN, top line), JJA (middle line) and SON (bottom line). Arrow width is an indication of the correlation strength between each variable. Correlations are calculated as per Figure 7. Correlations that are significantly different from expected (calculated using a block bootstrapping technique) are printed in bold italics.

During the most recent 1970–2009 subperiod, the main influence on SEA rainfall appears to have been the DMI, expressed particularly in annual and MAM values (MAM not shown). This was seen in the increased correlations between the DMI and MSLP as well as an increase in the annual correlation between DMI and RAIN. The NINO3.4–RAIN relationship in JJA returned to a similar strength to that observed in 1871–1909 (as seen in the regular correlations shown in Table 4), while the MSLP–RAIN relationship during JJA remained strong, but not quite as strong as during 1920–1959.

Repeating the subperiod path analysis using 20CR data (not shown) verified the correlations obtained using observational data, even in the early 1871–1909 period. Both datasets identified a weak relationship between MSLP and RAIN during 1871–1909, and an increase in the annual DMI–RAIN relationship from the first subperiod to the third. The annual DMI–MSLP relationship was also negative during 1920–1959 and strongly positive during 1970–2009 using both observational and 20CR data. Finally, both datasets revealed a drop in the NINO3.4–RAIN relationship in JJA during 1920–1959 and an increase in the DMI–RAIN and MSLP–RAIN correlations.

5. Discussion

It is clear that the relationships between SEA climate variables, ENSO and the IOD have varied considerably over 1871–2009. However, the majority of the correlations in Figure 8 are within the range possible due to natural variability, and the correlations that are significantly different do not provide a coherent indication of significant change. Given that there are 81 correlations shown in Figure 8, about eight correlations would be expected to be significant outside the 5–95% level just for random data. As there are only four correlations that are significantly different from expected, we suggest that the variations in the relationships between SEA climate, ENSO and the IOD over 1871–2009 years are within the range of natural variability. Importantly, correlations seen in the recent period, in the presence of background warming, do not appear to be significantly different from normal in the context of the last 140 years.

The largest variations in correlations between SEA rainfall and large-scale circulation features are identified during 1920–1959, when the relationship between NINO3.4 and SEA rainfall in austral winter became very weak, and the DMI was weakly negatively correlated with SEA MSLP and RAIN. A drop in global ENSO teleconnections during the first half of the 20th century has also been identified in previous studies (e.g. Elliott and Angell, 1988; Knippertz *et al.*, 2003; Suppiah, 2004), supporting this result.

The reversal in the normally positive IOD–SEA climate relationship may be related to an increase in easterly geostrophic flow and associated moisture flux over SEA during the 1940–1960 period, as reported by Rakich *et al.* (2008). The increased easterly flow may have led to a displacement of the Rossby wave train that is initiated in the eastern Indian Ocean and links the IOD to SEA rainfall (Cai and Cowan, 2008; Cai *et al.*, 2011). Another possibility is that the decrease in ENSO variance during 1920–1959 may have altered the behaviour of the IOD during this time, as ENSO is known to be a driving force in Indian Ocean temperature variations (Abram *et al.*, 2008; Dommenget, 2011).

With the decrease in the influence of NINO3.4 on SEA rainfall during 1920–1959, it is logical that the IOD and particularly local variations in MSLP would have played an increasing role in modulating the regional rainfall during this time. This is especially apparent during JJA (Figure 8). It is therefore interesting that the annual influence of the DMI on SEA rainfall and MSLP remained strong in the recent 1970–2009 period even when the correlations between NINO3.4 and RAIN, and NINO3.4 and MSLP increased. The JJA DMI–RAIN correlations returned to almost zero, but the annual correlations during the three subperiods clearly show an increase over time. The post-1960 period was dominated by more positive IOD events than any other period since 1880, most likely due to asymmetric warming in the Indian Ocean basin (Ihara *et al.*, 2008; Cai *et al.*, 2009). Ummenhofer *et al.* (2011) also suggest that positive IOD events are more related to dry conditions in SEA than negative events are related to wet condition. This nonlinear teleconnection may have resulted in the increased DMI–RAIN correlations seen in the 1970–2009 period.

Figures 7 and 8 also show that the local MSLP over SEA is influenced by both NINO3.4 and the DMI. As the MSLP variations are highly correlated with the intensity of the STR, and STR-I has been increasing in recent decades (Larsen and Nicholls, 2009), it is worth considering how these relationships may change in the future. The DMI showed particularly high correlations with MSLP during the recent 1970–2009 period, suggesting that the increased frequency of positive IOD events could also be linked to an increase in STR-I. It is important to remember also that the correlations in this study were calculated between detrended data using year-to-year differences, so the increasing relationship between MSLP and the DMI is not due to a common positive trend.

One relationship that has remained stable over the three subperiods is that between SEA rainfall and temperature, both Tmax and Tmin. Small decreases in Tmax–Tmin and Tmax–RAIN correlations were apparent in 1871–1909 but this is likely due to uncertainties associated with data quality and coverage (Ashcroft *et al.*, 2012). This result is in agreement with that of Trenberth and Shea (2005) who found no change in the relationship between mean temperature and precipitation variations on a global scale in the presence of large-scale warming.

The DMI–NINO3.4 relationship has also remained relatively stable over time, in contrast to previous research suggesting a decoupling of ENSO and the IOD during 1920–1959 (Abram *et al.*, 2008; Ihara *et al.*, 2008). The high agreement between the two indices may have led

to an underestimation of the role of each circulation feature in the path analysis. As noted by Risbey *et al.* (2009a), partial and semipartial correlations can act to weaken the apparent influence of one variable on another if the external variable and the variable of interest operate in a similar way. Partial and semipartial correlations also assume a linear relationship between different variables, which may mask important nonlinear elements of the relationships between ENSO, the IOD and SEA rainfall (Power *et al.*, 2006; Meyers *et al.*, 2007; Ummenhofer *et al.*, 2011). Nonetheless, the path analysis approach has isolated several important features of the roles played by ENSO, IOD and local MSLP in modulating SEA climate, and how these roles have changed over time.

Finally, the quality of pre-1910 data must also be considered in any study examining long-term changes in climatic behaviour. While the 1860–1909 temperature, MSLP and rainfall data for SEA have undergone detailed quality control and homogenization (Section 2), there may still be remaining issues in the early period due to fewer stations and less station history information. Similarly, the SST data used to calculate the DMI and NINO3.4 index have issues of spatial coverage in the pre-1900 period and during World War II (1939–1945) when ship observations were scarce and the methods used to record SST were uncertain (Kennedy *et al.*, 2011). However, the good agreement between the SEA observational dataset and the 20CR data increases confidence in the results presented in this study.

6. Conclusions

Newly extended datasets of temperature, rainfall and MSLP variations for SEA from 1860 to 2009 have been developed, allowing for the first instrumental examination of SEA climate over the past 150 years. The datasets have identified periods of cool, wet conditions in 1860–1864, 1870–1875 and 1891–1984 and dry, generally warm, conditions in 1876–1878, 1880–1885 and during the Federation Drought (1895–1902). Similar results were obtained using the 20CR, verifying our analysis of the newly extended observational network. The good agreement between the 20CR and observational data also shows that the 20CR is able to capture interannual variability in the SEA region from the late 19th century.

The relationships between SEA temperature, rainfall, MSLP and large-scale circulation features ENSO and the IOD were then examined using a path analysis based on the physical interactions between each variable. Strong relationships were identified between maximum temperatures in SEA and rainfall variations, while minimum temperatures showed seasonally varying links with Tmax and well as rainfall. SEA rainfall was found to be influenced by local MSLP variations, and rainfall and MSLP were modulated by changes in ENSO and the IOD. Interestingly, our analysis suggests that almost all of the IOD influence on SEA rainfall manifests as changes in regional MSLP, with the correlations between the IOD and SEA rainfall decreasing to almost zero when the common ENSO signal was removed. This result is in agreement with Dommenget (2011) and others (e.g. Allan *et al.*, 2001) who question the independence of the IOD.

An examination of changes in these relationships over three subperiods revealed that the influence of large-scale circulation features on the SEA climate has varied considerably over time, but that these variations are within the range of natural variability. While the non-stationary influence of ENSO on Australian rainfall is well-known (Kestin *et al.*, 1998; Power *et al.*, 1999), path analysis has provided additional information about the changes in ENSO–SEA climate relationship. In particular, the 1920–1959 period showed large changes in the correlations between SEA rainfall, ENSO, IOD and regional MSLP when compared to 1871–1909 and 1970–2009. Conversely, the interannual relationships between SEA temperature and rainfall have remained relatively stable during periods of changing remote influences on SEA rainfall and in the presence of large-scale warming. Similar results were again obtained using 20CR data, suggesting that the 20CR is able to represent important teleconnection patterns in the SEA region.

The extension of regional temperature, rainfall and MSLP data back to 1860 has allowed for a comparison between the modern climate, and climate during the second half of the 19th century, when ENSO and IOD variance was similar to today's but there was no significant increase in global temperatures (Jones *et al.*, 2012). Since the behaviour of ENSO is important for SEA seasonal forecasting and long-term climate prediction (Power and Smith, 2007), identifying changes in the ENSO and IOD teleconnections that may be due to anthropogenic climate change is vital. Our results suggest that recent changes in the influence of ENSO and the IOD on SEA rainfall variation lie within the range of natural variability experienced over the last 140 years.

Further study is now required to examine the role of low-frequency patterns such as the Interdecadal Pacific Oscillation in modulating SEA climate relationships (Power *et al.*, 1999; Gergis *et al.*, 2012). It would also be valuable to assess the influence of the SAM in future path analysis, particularly as increases in the SAM have been linked to recent drying in southern Australia (Hendon *et al.*, 2007; Nicholls, 2010). Unfortunately, current instrumental records of SAM variations are generally limited to the second half of the 20th century due to poor data coverage of the Antarctic region (Marshall, 2003). Given the large spatial variability of SEA rainfall, similar path analyses conducted for various subregions of SEA would also yield valuable information, although was considered beyond the scope of this study. A detailed examination of upper level conditions using extended reanalysis or model data would also improve understanding of the physical changes behind the variations identified in this analysis.

Acknowledgements

Thanks to Betrand Timbal, Robert Fawcett and Wasyl Drosdowsky (Australian Bureau of Meteorology) for

providing their STR-I and extended SEA rainfall data, and Gil Compo and Doug Schuster (National Ocean and Atmospheric Administration) for their valuable assistance with the 20th Century Reanalysis data. Many thanks also to Betrand Timbal, Neville Nicholls and two anonymous reviewers for their helpful comments. This research was funded by Australian Research Council (ARC) Linkage Project LP0990151.

References

Abram NJ, Gagan MK, Cole JE, Hantoro WS, Mudelsee M. 2008. Recent intensification of tropical climate variability in the Indian Ocean. *Nat. Geosci.* **1**: 849–853.

Alexander LV, Hope P, Collins D, Trewin B, Lynch A, Nicholls N. 2007. Trends in Australia's climate means and extremes: a global context. *Aust. Meteorol. Mag.* **56**(1): 1–18.

Alexander LV, Uotila P, Nicholls N, Lynch A. 2010. A new daily pressure dataset for Australia and its application to the assessment of changes in synoptic patterns during the last century. *J. Climate* **23**: 1111–1126.

Allan RJ, Chambers D, Drosdowsky W, Hendon H, Latif M, Nicholls N, Smith I, Stone RC, Tourre Y. 2001. Is there an Indian Ocean dipole and is it independent of the El Niño-Southern Oscillation? *CLIVAR Exch.* **6**(3): 18–22.

Allan RJ, Nicholls N, Jones PD, Butterworth IJ. 1991. A further extension of the Tahiti-Darwin SOI, early ENSO events and Darwin pressure. *J. Climate* **4**: 743–752, DOI: 10.1175/1520-0442

Ashcroft L, Karoly DJ, Gergis J. 2012. Temperature variations of southeastern Australia, 1860–2011. *Aust. Meteorol. Oceanogr. J.* **62**: 227–245.

Ashok K, Guan Z. 2003. Influence of the Indian Ocean Dipole on the Australian winter rainfall. *Geophys. Res. Lett.* **30**(15): 1821, DOI: 10.1029/2003GL017926

Australian Bureau of Meteorology. 2000. Australian Data Archive for Meteorology. *Climate Data Online*. http://www.bom.gov.au/climate/cdo/images/about/ADAM.pdf. Accessed 2011.

Australian Bureau of Meteorology. 2011. Southern Oscillation Index (SOI) Archives. *Australian Bureau of Meteorology*. http://reg.bom.gov.au/climate/current/soihtm1.shtml. Accessed August 25, 2011.

Australian Bureau of Meteorology. 2012. Annual Climate Summary 2011. *Australian Bureau of Meteorology*, 17. http://www.bom.gov.au/climate/annual_sum/annsum.shtml. Accessed June 1, 2012.

Barring L, Jonsson P, Achberger C, Ekstrom M, Alexandersson H. 1999. The Lund instrumental record of meteorological observations: reconstruction of monthly sea-level pressure 1780–1997. *Int. J. Climatol.* **19**(13): 1427–1443.

Behera S, Yamagata T. 2003. Influence of the Indian Ocean dipole on the Southern Oscillation. *J. Meteor. Soc. Jpn.* **81**(1): 169–177.

Cai W, Cowan T. 2008. Dynamics of late autumn rainfall reduction over southeastern Australia. *Geophys. Res. Lett.* **35**(9): L09708, DOI: 10.1029/2008GL033727

Cai W, Cowan T, Sullivan A. 2009. Recent unprecedented skewness towards positive Indian Ocean Dipole occurrences and its impact on Australian rainfall. *Geophys. Res. Lett.* **36**: L11705, DOI: 10.1029/2009GL037604

Cai W, van Rensch P, Cowan T. 2011. Teleconnection pathways of ENSO and the IOD and the mechanisms for impacts on Australian rainfall. *J. Climate* **24**: 3910–3923.

Compo GP, Whitaker JS, Sardeshmukh PD, Matsui N, Allan RJ, Yin X, Gleason BE, Vose RS, Rutledge G, Bessemoulin P, Brönnimann S, Brunet M, Crouthamel RI, Grant AN, Groisman PY, Jones PD, Kruk M, Kruger AC, Marshall GJ, Maugeri M, Mok HY, Nordli Ø, Ross TF, Trigo RM, Wang XL, Woodruff SD, Worley SJ. 2011. The Twentieth Century Reanalysis project. *Q. J. Roy. Meteorol. Soc.* **137**: 1–28.

CSIRO and the Australian Bureau of Meteorology. 2012. State of the Climate 2012. *CSIRO Resources*. http://wwwcsiroau/resources/State-of-the-Climatehtml. Accessed May 15, 2012.

Della-Marta P, Collins D, Braganza K. 2004. Updating Australia's high-quality annual temperature dataset. *Aust. Meteorol. Mag.* **53**: 75–93.

Dommenget D. 2011. An objective analysis of the observed spatial structure of the tropical Indian Ocean SST variability. *Climate Dynam.* **36**: 2129–2145, DOI: 10.1007/s00382-101-0787-1

Drosdowsky W. 2005. The latitude of the subtropical ridge over eastern Australia: The *L* index revisited. *Int. J. Climatol.* **25**(10): 1291–1299, DOI: 10.1002/joc.1196

Elliott WP, Angell JK. 1988. Evidence for changes in Southern Oscillation relationships during the last 100 years. *J. Climate* **1**(7): 729–737, DOI: 10.1175/1520-0442

Garden D. 2009. *Droughts, Floods and Cyclones*. Australian Scholarly Publishing: Melbourne, Australia.

Gergis JL, Fowler AM. 2005. Classification of synchronous oceanic and atmospheric El Niño-Southern Oscillation (ENSO) events for palaeoclimate reconstruction. *Int. J. Climatol.* **25**(12): 1541–1565, DOI: 10.1002/joc.1202

Gergis J, Ashcroft L. 2012. A rainfall history of southeastern Australia Part 2: a comparison of documentary, early instrumental and palaeoclimate records, 1788–2008. *Int. J. Climatol*., DOI: 10.1002/joc.3639

Gergis J, Fowler A. 2009. A history of El Niño–Southern Oscillation (ENSO) events since A.D. 1525: implications for future climate change. *Clim. Change* **92**(3): 343–387.

Gergis J, Gallant A, Braganza K, Karoly DJ, Allen K, Cullen L, D'Arrigo R, Goodwin I, Grierson P, McGregor S. 2012. On the long-term context of the 1997–2009 "Big Dry" in south-eastern Australia: insights from a 206-year multi-proxy rainfall reconstruction. *Clim. Change* **111**(3): 923–944, DOI: 10.1007/s10584-011-0263-x

Gillett N, Kell T, Jones PD. 2006. Regional climate impacts of the Southern Annular Mode. *Geophys. Res. Lett.* **33**: L23704.

Halpert MS, Ropelewski CF. 1992. Surface-temperature patterns associated with the Southern Oscillation. *J. Climate* **5**(6): 577–593, DOI: 10.1175/1520-0442

Hendon HH, Thompson DWJ, Wheeler MC. 2007. Australian rainfall and surface temperature variations associated with the Southern Hemisphere annular mode. *J. Climate* **20**(11): 2452–2467, DOI: 10.1175/JCLI4134.1

Hope P, Timbal B, Fawcett R. 2010. Associations between rainfall variability in the southwest and southeast of Australia and their evolution through time. *Int. J. Climatol.* **30**: 1360–1371.

Ihara C, Kushnir Y, Cane MA. 2008. Warming trend of the Indian Ocean SST and Indian Ocean dipole from 1880 to 2004*. *J. Climate* **21**: 2035–2046.

Jones DA. 1999. Characteristics of Australian land surface temperature variability. *Theor. Appl. Climatol.* **63**(1): 11–31, DOI: 10.1007/s007040050088

Jones DA, Trewin B. 2000. On the relationships between the El Niño–Southern Oscillation and Australian land surface temperature. *Int. J. Climatol.* **20**(7): 697–719, DOI: 10.1002/1097-0088

Jones DA, Wang W, Fawcett R. 2009. High-quality spatial climate data-sets for Australia. *Aust. Meteorol. Oceanogr. J.* **58**(4): 233–248.

Jones PD, Lister DH, Osborn TJ, Harpham C, Salmon M, Morice CP. 2012. Hemispheric and large-scale land-surface air temperature variations: an extensive revision and an update to 2010. *J. Geophys. Res.* **117**(D5), DOI: 10.1029/2011JD017139

Karoly DJ, Braganza K. 2005. Attribution of recent temperature changes in the Australian region. *J. Climate* **18**(3): 457–464, DOI: 10.1175/JCLI-3265.1

Karoly DJ, Hope P, Jones P. 1996. Decadal variations of the Southern Hemisphere circulation. *Int. J. Climatol.* **16**: 723–738.

Kennedy JJ, Rayner NA, Smith RO, Parker DE, Saunby M. 2011. Reassessing biases and other uncertainties in sea surface temperature observations measured *in situ* since 1850, part 2: biases and homogenisation. *J. Geophys. Res.* **116**(D14): D14104, DOI: 10.1029/2010JD015220

Kestin TS, Karoly DJ, Yano J-I, Rayner NA. 1998. Time-frequency variability of ENSO and stochastic simulations. *J. Climate* **11**(9): 2258–2272, DOI: 10.1175/1520-0442

Knippertz P, Ulbrich U, Marques F, Corte-Real JO. 2003. Decadal changes in the link between El Niño and springtime North Atlantic Oscillation and European-North African rainfall. *Int. J. Climatol.* **23**(11): 1293–1311, DOI: 10.1002/joc.944

Larsen SH, Nicholls N. 2009. Southern Australian rainfall and the subtropical ridge: variations, interrelationships, and trends. *Geophys. Res. Lett.* **36**, DOI: 10.1029/2009GL037786

Lavery B, Joung G, Nicholls N. 1997. An extended high-quality historical rainfall dataset for Australia. *Aust. Meteorol. Mag.* **46**: 27–38.

Livezey R, Chen WY. 1983. Statistical field significance and its determination by Monte Carlo techniques (in meteorology). *Mon. Weather Rev.* **111**: 46–59.
Marshall GJ. 2003. Trends in the Southern Annular Mode from observations and reanalyses. *J. Climate* **16**: 4134–4143.
McBride J, Nicholls N. 1983. Seasonal relationships between Australian rainfall and the Southern Oscillation. *Mon. Weather Rev.* **111**: 1998–2004.
Meneghini B, Simmonds I, Smith IN. 2006. Association between Australian rainfall and the Southern Annular Mode. *Int. J. Climatol.* **27**(1): 109–121, DOI: 10.1002/joc.1370
Meyers G, McIntosh P, Pigot L, Pook M. 2007. The years of El Niño, La Niña, and interactions with the tropical Indian Ocean. *J. Climate* **20**(13): 2872–2880, DOI: 10.1175/JCLI4152.1
Murphy B, Timbal B. 2008. A review of recent climate variability and climate change in southeastern Australia. *Int. J. Climatol.* **28**: 859–879.
Nicholls N. 1988. More on early ENSOs: evidence from Australian documentary sources. *Bull. Am. Meteorol. Soc.* **69**(1): 4–6.
Nicholls N. 1995. The centennial drought. In *Windows on Meteorology: Australian Perspective*, Webb EK (ed). CSIRO: Collingwood, Australia; 118–126.
Nicholls N. 2006. Detecting and attributing Australian climate change: a review. *Aust. Meteorol. Mag.* **55**: 199–211.
Nicholls N. 2010. Local and remote causes of the southern Australian autumn-winter rainfall decline, 1958–2007. *Climate Dynam.* **34**(6): 835–845, DOI: 10.1007/s00382-009-0527-6
Nicholls N, Drosdowsky W, Lavery B. 1996a. Australian rainfall variability and change. *Weather* **52**: 66–72.
Nicholls N, Lavery B, Frederiksen C, Drosdowsky W, Torok S. 1996b. Recent apparent changes in relationships between the El Niño Southern Oscillation and Australian rainfall and temperature. *Geophys. Res. Lett.* **23**(23): 3357–3360, DOI: 10.1029/96gl03166
Power S, Casey T, Folland C, Colman A. 1999. Inter-decadal modulation of the impact of ENSO on Australia. *Climate Dynam.* **15**: 319–324.
Power S, Haylock M, Colman R, Wang XD. 2006. The predictability of interdecadal changes in ENSO activity and ENSO teleconnections. *J Climate* **19**(19): 4755–4771, DOI: 10.1175/jcli3868.1
Power S, Smith IN. 2007. Weakening of the Walker Circulation and apparent dominance of El Niño both reach record levels, but has ENSO really changed? *Geophys. Res. Lett.* **34**: –L18702, DOI: 10.1029/2007GL030854
Power S, Tseitkin F, Torok SJ, Lavery B, Dahni R, McAveny B. 1998. Australian temperature, Australian rainfall and the Southern Oscillation, 1910–1992: coherent variability and recent changes. *Aust. Meteorol. Mag.* **47**: 85–101.
Rakich C, Holbrook N, Timbal B. 2008. A pressure gradient metric capturing planetary-scale influences on eastern Australian rainfall. *Geophys. Res. Lett.* **35**: L08713.
Rayner NA, Parker DE, Horton EB, Folland CK, Alexander LV, Rowell DP, Kent EC, Kaplan A. 2003. Global analyses of sea surface temperature, sea ice, and night marine air temperature since the late nineteenth century. *J. Geophys. Res.* **108**(D14): 4407, DOI: 10.1029/2002jd002670
Reason CJC, Allan RJ, Lindesay JA. 1998. Climate variability on decadal time scales: mechanisms and implications for climate change. *Palaeoclimates* **3**(1–3): 25–49.
Reynolds RW, Smith TM. 1994. Improved global sea surface temperature analyses using optimum interpolation. *J. Climate* **7**: 929–948.
Risbey JS, Pook MJ, McIntosh PC, Wheeler MC, Hendon HH. 2009a. On the remote drivers of rainfall variability in Australia. *Mon. Weather Rev*. **137**: 3233–3253.
Risbey JS, Pook MJ, McIntosh PC, Ummenhofer CC, Meyers G. 2009b. Characteristics and variability of synoptic features associated with cool season rainfall in southeastern Australia. *Int. J. Climatol*. **29**(11): 1595–1613, DOI: 10.1002/joc.1775
Ropelewski CF, Jones PD. 1987. An extension of the Tahiti-Darwin Southern Oscillation Index. *Mon. Weather Rev.* **115**(9): 2161–2165.
Saji NH, Goswami BN, Vinayachandran PN, Yamagata T. 1999. A dipole mode in the tropical Indian Ocean. *Nature* **401**(6751): 360–363.
Saji NH, Yamagata T. 2003. Possible impacts of Indian Ocean dipole mode events on global climate. *Climate Res.* **25**: 151–169.
Sartore G, Kelly B, Stain H, Albrecht G. 2008. Control, uncertainty, and expectations for the future: a qualitative study of the impact of the drought on a rural Australian community. *Rural Remote Health* **8**: 950.
Schumacker RE, Lomax RG. 2004. *A Beginner's Guide to Structural Equation Modeling*. Lawrence Erlbaun Associates: Mahwah, NJ.
Sturman A, Tapper N. 2004. *The Weather and Climate of Australia and New Zealand*. Oxford University Press: South Melbourne, Australia.
Suppiah R. 2004. Trends in the southern oscillation phenomenon and Australian rainfall and changes in their relationship. *Int. J. Climatol.* **24**: 269–290.
Thiessen AH. 1911. Precipitation averages for large areas. *Mon. Weather Rev.* **39**(7): 1082–1089, DOI: 10.1175/1520-0493
Timbal B, Arblaster J, Braganza K, Fernandez E, Hendon H, Murphy B, Raupach M, Rakich C, Smith I, Whan K, Wheeler M. 2010. *Understanding the Anthropogenic Nature of the Observed Rainfall Decline Across South-Eastern Australia*. CAWCR Technical Report No. 26. Day KA (ed). The Centre for Australian Weather and Climate Research, Melbourne, 180 pp.
Timbal B, Drosdowsky W. 2013. The relationship between the decline of southeastern Australian rainfall and the strengthening of the subtropical ridge. *Int. J. Climatol.* **33**(4): 1021–1034, DOI: 10.1002/joc.3492
Timbal B, Fawcett R. 2012. A historical perspective on south-eastern Australia rainfall since 1865 using the instrumental record. *J. Climate* **26**: 1112–1129, DOI: 10.1175/JCLI-D-12-00082.1
Torok S, Nicholls N. 1996. A historical annual temperature dataset for Australia. *Aust. Meteorol. Mag.* **45**: 251–260.
Trenberth KE. 1997. The definition of El Niño. *Bull. Am. Meteorol. Soc.* **78**(12): 2771–2777, DOI: 10.1175/1520-0477
Trenberth KE, Jones PD, Ambenje P, Bojariu R, Easterling D, Klein Tank AMG, Parker D, Rahimzadeh F, Renwick JA, Rusticucci M, Soden B, Zhai P. 2007. Observations: surface and atmospheric climate change. In *Climate Change 2007: The Physical Science Basis. Contribution of Working Group I to the Fourth Assessment Report of the Intergovernmental Panel on Climate Change*. Cambridge University Press: Cambridge, United Kingdom.
Trenberth KE, Shea DJ. 2005. Relationships between precipitation and surface temperature. *Geophys. Res. Lett.* **32**(14): L14703.
Trenberth KE, Stepaniak DP. 2001. Indices of El Niño evolution. *J. Climate* **14**: 1697–1701.
Trewin B. 2010. Exposure, instrumentation, and observing practice effects on land temperature measurements. *Wiley Interdiscip. Rev. Clim. Change* **1**(4): 490–506, DOI: 10.1002/wcc.46
Trewin B. 2013. A daily homogenized temperature data set for Australia. *Int. J. Climatol.* **33**(6): 1510–1529, DOI: 10.1002/joc.3530
Ummenhofer CC, Gupta AS, Briggs PR, England MH, McIntosh PC, Meyers GA, Pook MJ, Raupach MR, Risbey JS. 2011. Indian and Pacific Ocean influences on southeast Australian drought and soil moisture. *J. Climate* **24**: 1313–1336, DOI: 10.1175/2010JCLI3475.1
Verdon-Kidd DC, Kiem AS. 2009. Nature and causes of protracted droughts in southeast Australia: comparison between the Federation, WWII, and Big Dry droughts. *Geophys. Res. Lett.* **36**(22): L22707, DOI: 10.1029/2009GL041067
Wang XL. 2008. Penalized maximal *F* test for detecting undocumented mean shift without trend change. *J. Atmos. Oceanic Tech.* **25**(3): 368–384, DOI: 10.1175/2007JTECHA982.1
Wang XL, Fang Y. 2010. *RHtestsV3 User Manual*. Atmospheric Science and Technology Directorate, Science and Technology Branch, Environment Canada, Toronto. http://cccma.seos.uvic.ca/ETCCDMI/software.shtml. Accessed August 15, 2010.
Wang XL, Feng Y. 2010. *RHtestsV3 User Manual*. Atmospheric Science and Technology Directorate, Science and Technology Branch, Environment Canada, Toronto. 26 pp. http://cccma.seos.uvic.ca/ETCCDMI/software.shtml. Accessed August 15, 2010.
Wang XL, Wen QH, Wu Y. 2007. Penalized maximal *t* test for detecting undocumented mean change in climate data series. *J. Appl. Meteorol. Climatol.* **46**(6): 916–931, DOI: 10.1175/JAM2504.1
Wilks DS. 1995. *Statistical Methods in the Atmospheric Sciences: An Introduction*. Elsevier Academic Press: San Diego, CA.
Woodruff S, Worley SJ, Lubker S, Ji Z, Freeman E, Berry DI, Brohan P, Kent EC, Reynolds R, Smith SR, Wilkinson C. 2011. ICOADS Release 2.5: extensions and enhancements to the surface marine meteorological archive. *Int. J. Climatol.* **31**(7): 951–967, DOI: 10.1002/joc.2103
Yu J, Mechoso C, McWilliams J, Arakawa A. 2002. Impacts of the Indian Ocean on the ENSO cycle. *Geophys. Res. Lett.* **29**(8): 1204, DOI: 10.1029/2001GL014098
Zwiers FW, Zhang X, Feng Y. 2011. Anthropogenic influence on long return period daily temperature extremes at regional scales. *J. Climate* **24**(3): 881–892, DOI: 10.1175/2010JCLI3908.1

